Optimized Schwarz Methods with the Yin-Yang Grid for Shallow Water Equations

Abdessamad Qaddouri

Recherche en prévision numérique, Atmospheric Science and Technology Directorate, Environment Canada, Dorval, Québec, Canada.
abdessamad.qaddouri@ec.gc.ca

Summary. An efficient implementation of the Schwarz method is used to solve the 2D linear system of shallow-water equations (SWEs) on the sphere with an overset grid system named Yin-Yang. In this paper the convergence of optimized Schwarz method for solving an elliptic problem is increased by substructuring the algorithm in terms of interface unknowns. In this work we show, by numerical tests, that the use of the Yin-Yang grid avoids the "poles problems" resulting from the global latitude-longitude mesh convergence in the polar regions.

1 Introduction

The Yin-Yang overset grid (see Fig. 1) was suggested in [4] as a quasi-uniform grid free from the polar singularity. This grid system is constructed by overlapping two perpendicularly oriented identical parts of latitude-longitude grid. In [5] it was shown that the Schwarz domain decomposition method can be successfully applied to linear SWEs. In each subdomain the same system of equations is discretized by an implicit time method using the same time step where at each time step an elliptic problem is solved. In [5] this method was used to solve the 1D SWEs on the circle and the elliptic problem was solved by the iterative optimized Schwarz method (see [2] and references therein). In this paper we apply the same method to the 2D linear SWEs on the Yin-Yang grid. We show that it is possible to increase the convergence of the optimized Schwarz method for solving the elliptic problem by using the substructuring formulation. Because the two subgrids of the Yin-Yang grid do not match, the variable update at the subdomain interfaces is done by cubic Lagrange interpolation. The complete 2D linear SWE solutions on the Yin-Yang grid are compared to integrations using the spectral model on a Gaussian grid and a finite-difference model on a latitude-longitude grid. The paper is organized as follows: in Section 2, we present the 2D linear SWEs with their discretized form and solution method, in Section 3 the 2D positive definite Helmhotz problem is solved on the Yin-Yang grid, the solver is either an iterative formulation or an substructuring formulation of the optimized Schwarz method, in Section 4 numerical results are shown and finally concluding remarks are given in Section 5.

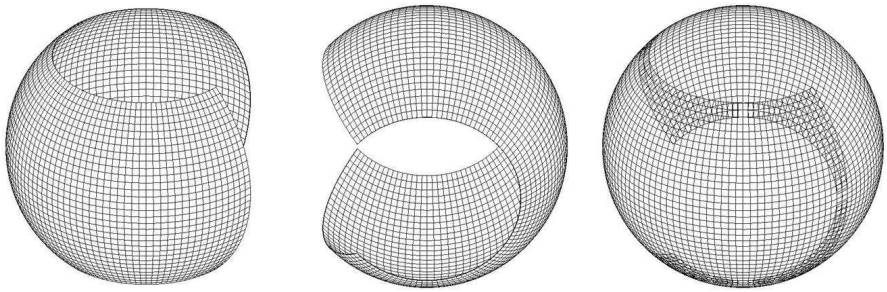

Fig. 1. Yin-Yang grid system. The Yang grid is shown on the left, the Yin grid in the middle, and their composition on the right

2 The 2D Linear Shallow Water Equations

In this section, we develop an implicit global linear shallow-water model on the sphere by using a domain decomposition method on Yin-Yang grid. The major goal of this work is the demonstration that this type of grid system removes the poles problems. Each of two component of Yin-Yang overset grid spans the Subregion S_l, $l = 1, 2$, defined by

$$S_{(l)} = \{(\lambda, \theta); \quad |\theta| \leq \frac{\pi}{4} + \delta \quad |\lambda| \leq \frac{3\pi}{4} + \delta\}, \tag{1}$$

where (λ, θ) are the longitude and the latitude with respect to the local cartesian referential (see [1]) and δ is the minimum overlap. The relationship between the Yin coordinate and Yang coordinate is denoted in cartesian coordinates by

$$(x_{(l)}, y_{(l)}, z_{(l)}) = (-x_{(3-l)}, z_{(3-l)}, y_{(3-l)}) \qquad l = 1, 2. \tag{2}$$

The governing equations for each subdomain l, $l = 1, 2$ are the linear SWEs on a non rotating sphere of radius a

$$\left[\frac{\partial U^{(l)}}{\partial t} + \frac{1}{a^2}\frac{\partial \phi^{(l)}}{\partial \lambda}\right] = 0, \tag{3}$$

$$\left[\frac{\partial V^{(l)}}{\partial t} + \frac{1}{a^2}\cos\theta\frac{\partial \phi^{(l)}}{\partial \theta}\right] = 0, \tag{4}$$

$$\left[\frac{\partial \phi^{(l)}}{\partial t} + \phi^* D^{(l)}\right] = 0, \tag{5}$$

where a is the Earth radius, (U, V) are the wind images [wind multiplied by $\frac{\cos\theta}{a}$], ϕ the perturbation geopotential from the reference geopotential ϕ^* and D is the divergence defined by

$$D = \frac{1}{\cos^2\theta}\left(\frac{\partial U}{\partial \lambda} + \cos\theta\frac{\partial V}{\partial \theta}\right). \tag{6}$$

The ϕ field gradient components and divergence D give rise to high frequency gravity waves. They are always integrated implicitly in time, enabling the use of a long time step Δt. A time discretization of equations (3)-(5) is

$$\left[\frac{U^{(l)}}{\tau}+\frac{1}{a^2}\frac{\partial\phi^{(l)}}{\partial\lambda}\right](\lambda,\theta,t)=R_U^{(l)}=\left[\frac{U^{(l)}}{\tau}-\frac{1}{a^2}\frac{\partial\phi^{(l)}}{\partial\lambda}\right](\lambda,\theta,t-\Delta t)\,, \tag{7}$$

$$\left[\frac{V^{(l)}}{\tau}+\frac{1}{a^2}\cos\theta\frac{\partial\phi^{(l)}}{\partial\theta}\right](\lambda,\theta,t)=R_V^{(l)}=\left[\frac{V^{(l)}}{\tau}-\frac{1}{a^2}cos\theta\frac{\partial\phi^{(l)}}{\partial\theta}\right](\lambda,\theta,t-\Delta t)\,, \tag{8}$$

$$\left[\frac{\phi^{(l)}}{\tau}+\phi^* D^{(l)}\right](\lambda,\theta,t)=R_{\phi^{(l)}}=\left[\frac{\phi^{(l)}}{\tau}-\phi^* D^{(l)}\right](\lambda,\theta,t-\Delta t)\,, \tag{9}$$

where $\tau=\Delta t/2$. As for the 1D SWEs in [5], the second order finite difference spatial discretization is done on a staggered Arakawa C grid [1] where the variables U, V and ϕ are carried at alternate points in space on (U-grid), ($v-$grid) and (ϕ-grid), respectively. We use (N,M) grid points for the scalar (ϕ-grid), (N-1,M) grid points for (U-grid) and (N,M-1) grid points for (V-grid). The discretized equations on each subdomain l are

$$\left[\frac{U_{i,j}^{(l)}}{\tau}+\frac{1}{a^2}\frac{\phi_{i+1,j}^{(l)}-\phi_{i,j}^{(l)}}{h_\lambda}\right]=R_U^{(l)},\quad i=1,N-1;j=1,M \tag{10}$$

$$\left[\frac{V_{i,j}^{(l)}}{\tau}+\frac{1}{a^2}\cos\theta_j\frac{\phi_{i,j+1}^{(l)}-\phi_{i,j}^{(l)}}{h_\theta}\right]=R_V^{(l)}\quad i=1,N;j=1,M-1 \tag{11}$$

$$\left[\frac{\phi_{i,j}^{(l)}}{\tau}+\phi^* D_{i,j}^{(l)}\right]=R_\phi^{(l)}\quad i=2,N-1;j=2,M-1 \tag{12}$$

with

$$D_{i,j}^{(l)}=\frac{1}{\cos^2\theta_j}\left(\frac{U_{i,j}^{(l)}-U_{i-1,j}^{(l)}}{h_\lambda}+\cos\theta_j\frac{V_{i,j}^{(l)}-V_{i,j-1}^{(l)}}{h_\theta}\right), \tag{13}$$

where h_λ, h_θ are the grid spacing along the longitudinal and latitudinal directions respectively. The resulting equations (10)-(12) are combined to obtain a single discretized elliptic equation (14) for ϕ which is solved by the optimized Schwarz method discussed in the following sub-sections, and the wind is updated by equations (3)-(4). Then given fields $U^{(l)}$, $V^{(l)}$ and $\phi^{(l)}$ at the previous time step, the solution method is summarized as follows:

- The right-hand sides $R_U^{(l)}$, $R_V^{(l)}$ and $R_\phi^{(l)}$ are calculated in parallel on the two subdomains.
- The elliptic problem is solved and the geopotential $\phi^{(l)}$ is updated on the two subdomains. Interpolation and communication are required to obtain values at subdomain interfaces.
- The wind vector fields ($U^{(l)}$,$V^{(l)}$) are updated in parallel on the two subdomains.

2.1 Iterative Formulation of the Optimized Schwarz Method

Similar to the classical Schwarz method, we solve the discretized problems iteratively in each subdomain

$$\begin{aligned}&-\frac{2+h_\theta\tan\theta_j}{2h_\theta^2}\phi_{i,j-1}^{(l),k}-\frac{1}{\cos^2\theta_j h_\lambda^2}\phi_{i-1,j}^{(l),k}+(\eta+\frac{2}{\cos^2\theta_j h_\lambda^2}+\frac{2}{h_\theta^2})\phi_{i,j}^{(l),k}\\&-\frac{1}{\cos^2\theta_j h_\lambda^2}\phi_{i+1,j}^{(l),k}-\frac{2-h_\theta\tan\theta_j}{2h_\theta^2}\phi_{i,j+1}^{(l),k}=R_{i,j}^{(l),k},\quad i=1,\ldots,N;\ j=1,\ldots,M,\end{aligned} \tag{14}$$

where $\eta = \frac{a}{\phi^* \Delta t^2}$ is a positive and constant parameter and R is the corresponding right-hand-side function. Following the ideas of [2], we use the following discretizations of the higher order transmission conditions on each interface $\Gamma_d^{(l)} (d = 1, \cdots 4)$

$$\frac{\partial \phi^{(l),k}}{\partial \nu_l} + \beta_d^{(l)} \phi^{(l),k} + \alpha_d^{(l)} \frac{\partial^2 \phi^{(l),k}}{\partial \tau_l^2} = \frac{\partial \phi^{(3-l),k-1}}{\partial \nu_l} + \beta_d^{(l)} \phi^{(3-l),k-1} + \alpha_d^{(l)} \frac{\partial^2 \phi^{(3-l),k-1}}{\partial \tau_l^2}. \tag{15}$$

The symbol $\frac{\partial}{\partial \nu_l}$ stands for the normal derivative of each subdomain and $\frac{\partial}{\partial \tau_l}$ is the corresponding tangential derivative. The $\alpha_d^{(l)}, \beta_d^{(l)}$ are real parameters introduced to optimize the performance of the method. We obtain these coefficients numerically, assuming the coefficients $\alpha_d^{(l)}$ and $\beta_d^{(l)}$ are independent of the boundary d and are antisymmetric, i.e.

$$\alpha_d^{(1)} = -\alpha_d^{(2)}, \quad \beta_d^{(1)} = -\beta_d^{(2)}. \tag{16}$$

In Fig. 2 we represent the performance for the solution of the elliptic problem where each subdomain consists of 90×30 grid points, the overlap δ is one grid point spacing and the Helmhotz coefficient η is equal to one. For the approximate optimal values of the parameters $\alpha_d^{(l)}$ and $\beta_d^{(l)}$, the corresponding methods (see Fig. 2) converge in a small number of iterations and the convergence is much better than the convergence of the classical Schwarz method. This gain more than compensates for the extra cost of computing the needed additional derivatives.

2.2 Substructuring Formulation of the Optimized Schwarz Method

It is possible to both increase the robustness of the optimized Schwarz method and its convergence speed by replacing the above fixed point iterative solver by a Krylov-type method (see [2] and references therein). This is made possible by substructuring the algorithm in terms of interface unknowns, that we denote here by $T_d^{(l)}$ for each subdomain l and interface d. We consider the substructuring formulation of the elliptic problem in equations (14)-(15) where the unknowns $T_d^{(l)}$ are equal to the right-hand side of equation (15), and we rewrite the problem to be solved on each subdomain as

$$\begin{aligned} A^{(l)} \phi^{(l)} &= R^{(l)} \\ B_d^{(l)} \phi^{(l)} &= B_d^{(l)} \phi^{(3-l)} = T_d^{(l)}, \end{aligned} \tag{17}$$

where $B_d^{(l)}$ is the transmission operator which is the identity in the case of Dirichlet conditions. In the previous iterative Schwarz method we solve iteratively, with iteration number $k = 1, \ldots, k_{max}$, in each subdomain the system of equations

$$A^{(l)} \phi^{(l),k} = R^{(l)} + B_d^{(l)} \phi^{(3-l),k-1} = R^{(l)} + T_d^{(l),k-1}, \tag{18}$$

where the matrix $A^{(l)}$ now includes the corrections from the transmission conditions. The Schwarz method corresponds then to the solution for the interface problem unknowns $T_d^{(l)}$ by the Jacobi algorithm

$$T_d^{(l),k} = B_d^{(l)} (A^{(3-l)})^{-1} T_d^{(3-l),k-1} + B_d^{(l)} (A^{(3-l)})^{-1} R^{(3-l)}. \tag{19}$$

We can improve the convergence by considering GMRES, or any other Krylov method, in order to solve the interface system of equations

$$\begin{bmatrix} I & -B_d^{(l)}(A^{(3-l)})^{-1} \\ -B_d^{(3-l)}(A^{(l)})^{-1} & I \end{bmatrix} \begin{bmatrix} T_d^{(l)} \\ T_d^{(3-l)} \end{bmatrix} = \begin{bmatrix} B_d^{(l)}(A^{(3-l)})^{-1}R^{(3-l)} \\ B_d^{(3-l)}(A^{(l)})^{-1}R^{(l)} \end{bmatrix}. \quad (20)$$

The spectral radius of the left-hand-side matrix in equation (20) depends on the choice of the interface conditions $B_d^{(l)}$. Once the interfaces functions $T_d^{(l)}$ are known, the subproblem solutions are updated in parallel. In Table 1 we consider the two interface equation solvers, Jacobi and GMRES, and we give the number of iterations so that the maximum error is smaller than 10^{-6}. We see that the optimized Robin or second-order transmission conditions give a significant improvement when using either solver.

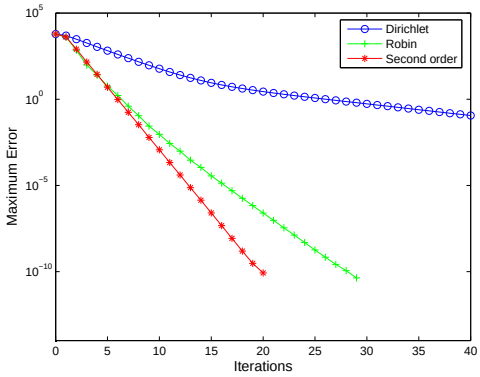

Fig. 2. Convergence behavior for the iterative classical Schwarz and the iterative optimized Schwarz methods, overlap $= 1h$ and $\eta = 1$

Table 1. Number of iterations for 3 interface conditions and 2 solvers. Each panel is 90×30, overlap$= 1h$ and $\eta = 1$.

Boundary Cond.	ASM	GMRES
Dirichlet	116	26
Robin	20	12
Second order	16	9

3 Numerical Results

In order to assess the capability of the Yin-Yang grid to alleviate the pole problem, we consider the solutions for the 2D linear SWEs on both a global latitude-longitude grid and the Yin-Yang grid and we compare them with a spectral model solution

which is free of the pole problem. We start from an initial state at rest (U and $V = 0$) with the initial geopotential perturbation given by:

$$\phi(\lambda, \theta, t = 0) = 2\ \Omega a u_0\ \sin^3(\theta)\cos(\theta)\sin(\lambda) \tag{21}$$

where $\Omega = 0.00007292 s^{-1}$, and $u_0 = 20 m/s$. If we expand ϕ in terms of truncated series of spherical harmonics, its spectrum shows that the non-zero contributions are only from total wavenumbers 2 and 4. We take a global lat-lon grid with the resolution 80 ×40, Yin-Yang grid with resolution 60×20 in each panel, and we compare with an equivalent spectral model with a truncation at wavenumber 39. There must be no interaction between the time tendencies of different spectral coefficients. No new spectral mode can appear during the evolution from the initial state. The spectrum (not plotted here) of the perturbation of the geopotential given by the 3 models after 4 hours shows that for the spectral model the only non zeros are the contributions from wavenumbers 2 and 4 and the initial energy, initially potential, is now divided into kinetic and potential parts. In the spectrum of the perturbation of the geopotential given by using the lat-lon grid and the Yin-Yang grid, there are non zero contributions from wavenumbers other than 2 and 4, however the energy at these wavenumbers is much smaller when using the Yin-Yang grid. We show in Fig. 3 the difference between the perturbation of the geopotential after 4 hours given by using the lat-lon and Yin-Yang gridpoint models and by the spectral model. For lat-lon we can see that the biggest difference is near the poles. The difference between the solution on the Yin-Yang grid and the spectral model is the same everywhere on the globe. The maximum difference after 24 hours (not shown here) between the Yin-Yang gridpoint model and the spectral model solutions corresponds to only 1 m height difference. We can conclude that the use of the quasi-uniform Yin-Yang grid eliminates the pole problem and gives much more accurate solutions than with the standard lat-lon grid.

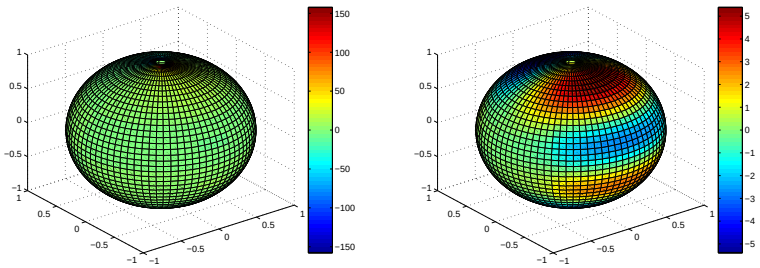

Fig. 3. Geopotential differences between spectral and Lat/lon (left), Yin-Yang and spectral (right). The two subfigures have not the same scale

4 Conclusion

In this paper we have shown that the Schwarz domain decomposition methods are practical for obtaining solutions of the linear SWEs on the sphere with the overset

grid system Yin-Yang. In a previous study [5] the convergence analysis of the 1D iterative solution of the elliptic problem on the circle yielded an analytical formula for the optimized coefficients of the transmission conditions. In this paper the optimized coefficients for the 2D case on the Yin-Yang grid were found numerically and it was possible to both increase the robustness of the optimized Schwarz method and its convergence speed by using the substructuring formulation. We have demonstrated that the use of the quasi-uniform Yin-Yang grid effectively eliminates the pole problem and gives more accurate solutions than when using the latitude-longitude grid.

We have not yet validated the full 2D SWEs model on the Yin-Yang grid, but 2D passive semi-Lagrangian advection has been thoroughly tested for this grid, see [5, 6], and the results were comparable to the value in [3]. In future work we will complete the validation of the SWEs with the Yin-Yang grid using the test set of Williamson et al. [7], and finally we will consider the Yin-Yang grid system with more than one regular subdomain in each panel.

Acknowledgement. This research was partly supported by the Canadian Foundation for Climate and Atmospheric Sciences through a grant to the QPF network and by the Office of Science (BER), U.S. Department of Energy, Grant No. DE-FG02-01ER63199. I would like to thank Jean Côté and Martin Gander for reviewing the manuscript.

References

[1] A. Arakawa and V. Lamb. Computational design of the basic dynamical processes of the ucla general circulation model. In *Methods in Computational Physics*, volume 17, pages 174–267. Academic Press, 1977.

[2] M. Gander. Optimized Schwarz methods. *SIAM J. Numer. Anal.*, 44(2):699–731, 2006.

[3] R. Jacob-Chien, J.J. Hack, and D.L. Williamson. Spectral transform solutions to shallow water test set. *J. Comput. Phys.*, 119:164–187, 1995.

[4] A. Kageyama and T. Sato. Yin-yang grid: An overset grid in spherical geometry. *Geochem. Geophys. Geosyst.*, 5(9), 2004.

[5] A. Qaddouri, J. Côté, M. Gander, and S. Loisel. Optimized Schwarz methods with an overset grid system for the shallow-water equations: Preliminary results. *Appl. Numer. Math.*, 2007. In press.

[6] A. Qaddouri, L. Laayouni, J. Côté, and M. Gander. Optimized Schwarz methods with an overset grid system for the shallow-water equations. *Research Activities in Atmospheric and Oceanic Modelling WMO/TD-1276*, 35(3):21–22, 2005.

[7] D.L. Williamson, J.B. Drake, J.J. Hack, R. Jacob-Chien, and P.N. Swarztrauber. A standard test set for numerical approximations to the shallow water equations in spherical geometry. *J. Comput. Phys.*, 102:211–224, 1992.